

Evaluation of the surface quality of spun materials using topothesy

Tomasz Blachowicz* and Michal Koruszowicz

Institute of Physics – Center for Science and Education, Silesian University of Technology, 44-100 Gliwice, Poland

*Corresponding author E-mail address: tomasz.blachowicz@polsl.pl

INFO

CDAPT, ISSN 2701-939X
Peer reviewed article
2021, Vol. 2, No. 2, pp. 208-216
DOI 10.25367/cdatp.2021.2.p208-216
Received: 27 November 2021
Accepted: 18 December 2021
Available online: 18 December 2021

ABSTRACT

Topothesy and fractal dimensions were calculated for poly(acrylonitrile) (PAN) nanofiber mats obtained by electrospinning. These methods enable quantitatively describing and thus comparing solid-state surfaces and detecting fabric errors. The obtained variety of structural properties results from different substrates and after-treatments, e.g. stabilization and carbonization. The change in spatial morphology was reported for different magnifications of images obtained with the use of helium ion microscopy (HIM).

Keywords

Surface analysis,
microscopic images,
fractals,
topothesy,
roughness of materials

© 2021 The authors. Published by CDAPT.

This is an open access article under the CC BY-NC-ND license
<https://creativecommons.org/licenses/> peer-review under
responsibility of the scientific committee of the CDAPT.

© 2021 CDAPT. All rights reserved.

1 Introduction

Analysis of surface and structural properties of textile materials, from the perspective of fractal-related investigations, can be realized by using image processing methods. In its common sense that the image processing approach relies on counting pixels for a given selected region. Importantly, in practice gray-scaled or even monochromatic one-bit photographs are elaborated. The selected region under investigation might be a circle, a rectangular or square area. Usually, the counting procedure is repeated in many places – selected at random or at regularly (sequentially) distributed locations. Finally, the collected information is properly elaborated, e.g. averaged, and the final set of characteristic parameters can be provided. We can mention here that there are plenty of universal approaches, such as fractal capacity dimension and fractal correlation dimensions [1], diffusive dimension and the associated random walk on images [2], succolarity [3], lacunarity [4], and finally topothesy [5], which is the main subject of this publication.

Topothesy is in use for many years as a testing method for solid-state surfaces, e.g. in metals after machining [6]. Thomas and Rosén explained that the fractal dimension is sufficient to describe self-

similar fractals, while real surfaces – which are not self-similar in mechanical or optical investigations – need the topothesy as an additional scaling parameter, which is defined as the in-plane distance along which the surface slope is one radian on the average [7,8]. Russ mentions that this distance can be very small in real samples, making the physical interpretation often complicated, but that the topothesy has the advantage that it can be evaluated from a line profile, like in mechanical surface roughness measurements [8]. This fractal parameter has been successfully implemented, e.g., for fingerprint detection [9].

On the other hand, there are only few computer-based approaches used in automated fabric defect detection systems, applying calculations of fractal parameters [10]. Hanmandlu *et al.*, e.g., reported on investigating torn fabrics, oil stains, miss picks and interlacing of two webs by topothesy and fractal dimension and found that these parameters did not only represent surface roughness, but also the self-similarity in the textures, enabling using them for detection of such visible errors where the self-similarity was changed [5]. Militký and Bajzík showed that fractal dimensions were related to surface roughness characteristics, as measured by Kawabata evaluation system [11]. Most other investigations of textile surfaces and fabric defects by mathematical methods concentrate on evaluations via the Hurst exponent [12], Sobel edge detection, thresholding methods [13], Gabor filters, wavelet transform and others [14].

Here, we want to employ topothesy for relatively large, magnified photographs of fibrous structures. After providing some theoretical examples of very simple cases, we will present results for poly(acrylonitrile) (PAN) nanofibers mats obtained by electrospinning [15].

2 Fractal characteristics and topothesy

As mentioned before, surface analysis in different methodologies can deal with gray-scaled or even 1-bit black-and-white maps. The topothesy tests the morphology of gray pixels in a range of intensities of $< 0; 255 >$. It counts the difference between the intensities of two selected regions per distance between them. This is why it is related to a slope and can be used for quantification of solid state roughness. The topothesy depends on the so-called spectral function $S(\tau)$ expressed as follows.

$$S(\tau) = \frac{1}{(m-\tau)^2} \sum_{i=1}^{m-\tau} \sum_{j=1}^{m-\tau} |g(i, j) - g(i + \tau, j + \tau)|, \quad (1)$$

where an image under analysis has the pixel size $(m \times m)$, τ is the testing range $< 1 < \tau < m - 1 >$ of the spectral function, and g is the gray-level value at a given pixel (i, j) . Thus, the obtained spectral function $S(\tau)$ is a measure of the average slope for the analyzed area. It was shown by J. C. Russ [16] that the spectral function can be represented by two fractal parameters, fractal dimension d and topothesy T , in the following way:

$$S(\tau) = \tau^{2(2-d)} T^{2(d-1)}. \quad (2)$$

This means that topothesy and spectral function are directly involved in the expression, which makes it suitable for fast calculations. For non-fractals and 2-dimensional objects, $d = 2$ and $S \sim T^2$. On the logarithmic scale, Eq. 2 can be expressed as a linear dependence, namely

$$\ln(S(\tau)) = 2(2 - d)\ln(\tau) + 2(d - 1)\ln(T). \quad (3)$$

This equation shows that topothesy can be deduced from the point of intersection of a tangent line with the plot at $\ln(\tau) = 0$. From the linear regression fit parameters $(a, b \text{ in } y = ax + b)$, we can calculate topothesy and fractal dimension:

$$T = \exp(b/(2 - a)) \text{ and } d = 2 - a/2. \quad (4)$$

In this paper we show investigations of square regions of size $(m \times m)$, e.g., the whole image or its parts, calculating linear fitting within the range of $\ln(\tau) = \langle 0.5; 1.5 \rangle$.

Before presentation of topothesy for fiber-based electrospun materials, we show some theoretical simple structures with different levels of spatial frequencies (Fig. 1) in order to make the reader more familiar with the $S(\tau)$ function and topothesy. Here we see that the topothesy shows larger values if the lines alternate on smaller scales.

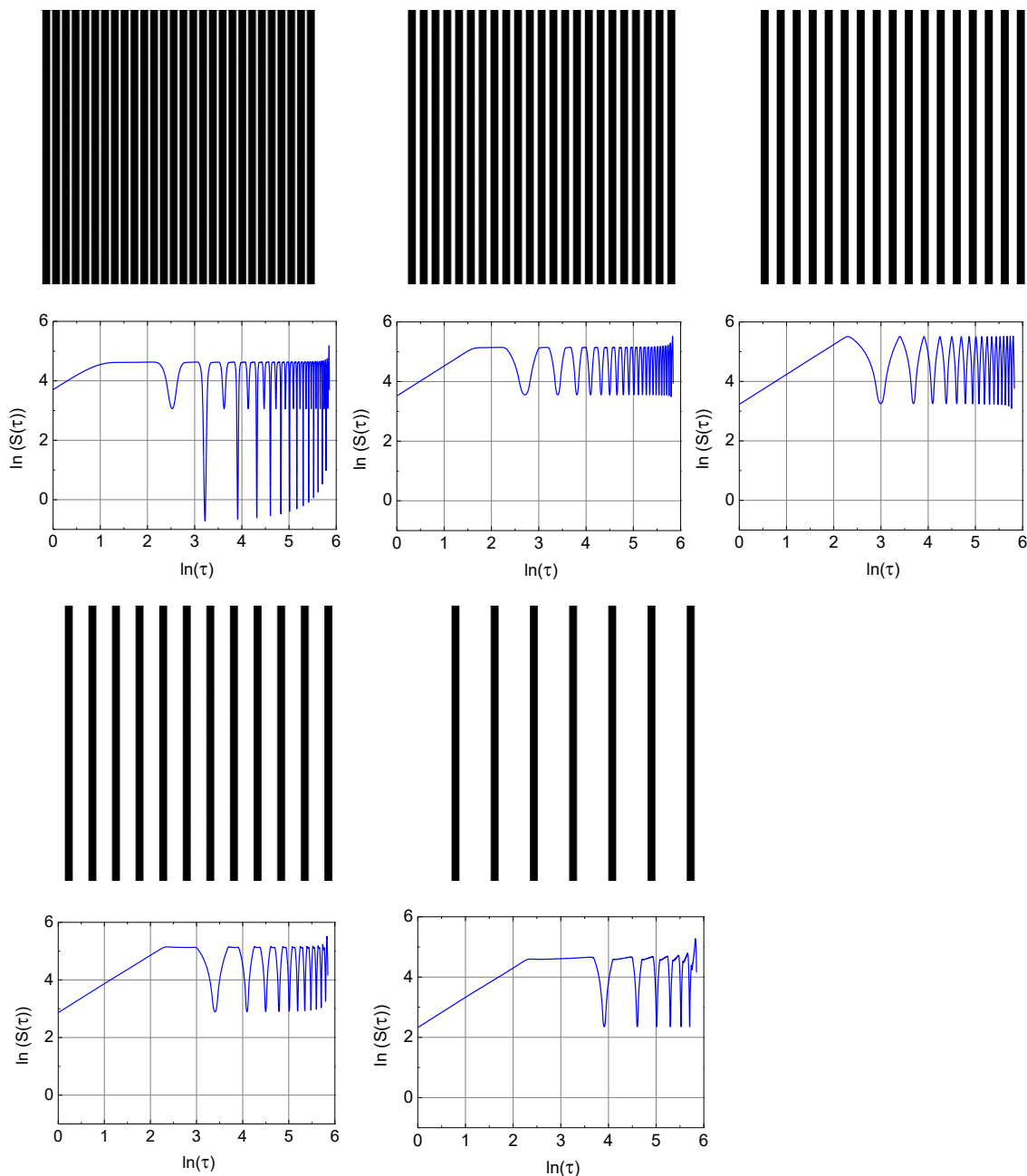


Fig. 1 Spectral functions calculated for bar structures with different ratios of bar width to the width of white space between them. For small values of $\ln(\tau)$ one can observe a linear function mentioned in Eq. 3. The smaller the value of the line intersection at $\ln(\tau) = 0$, the smaller is the topothesy.

A similar finding can be reported for irregularly placed dots instead of strips in identical distances, as visible in Fig. 2, while more comparable values of the topothesy can be found in continuously changing gray-scale images with different gradient orientations (Fig. 3).

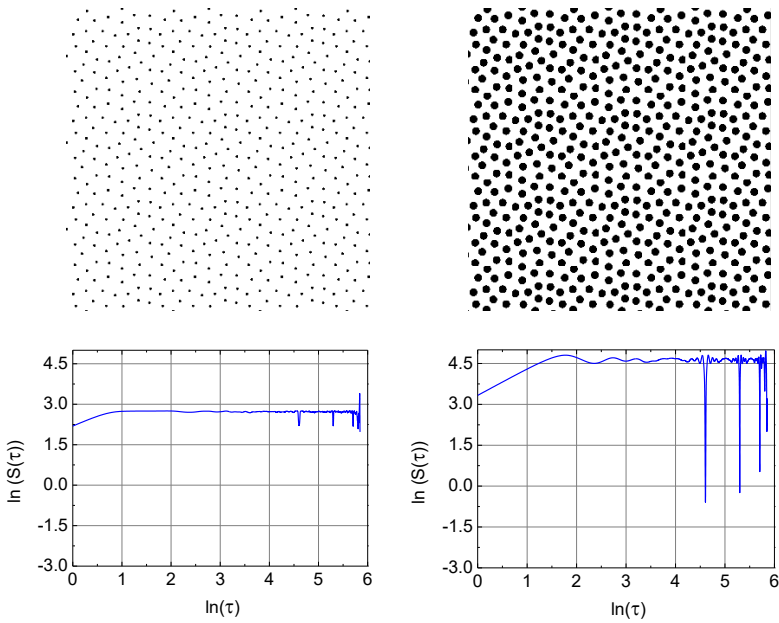


Fig. 2 Spectral functions of randomly distributed circles; small ones (on the left) and bigger ones (on the right). Topothesy of the left image is smaller, since white background dominates. Larger black circles on the right contribute more significantly to image non-uniformity.

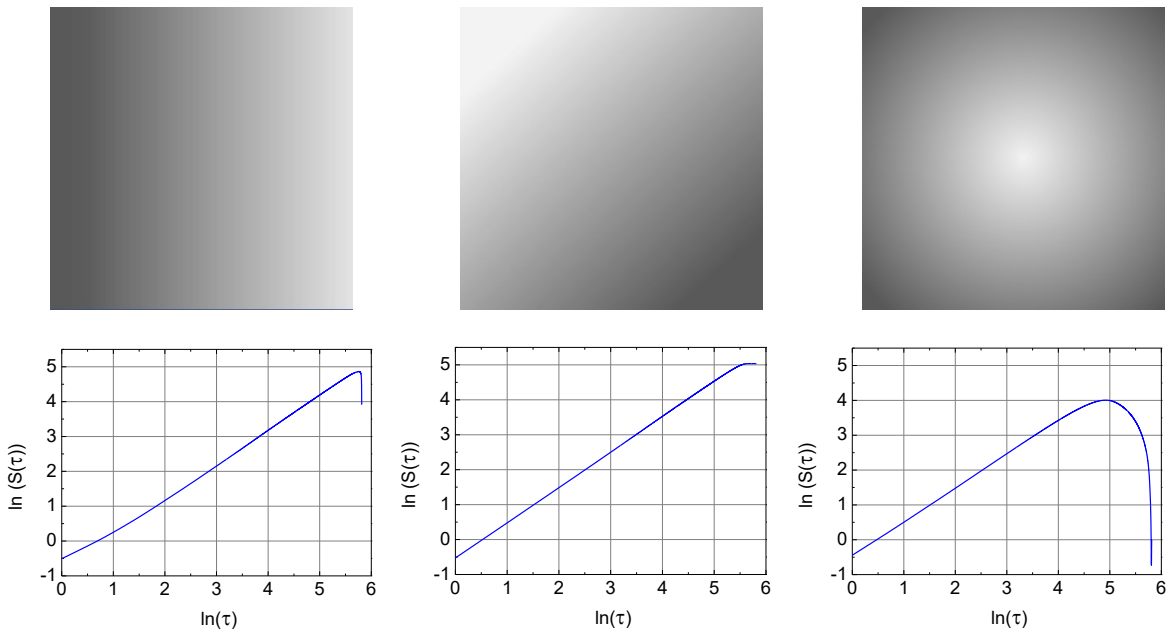


Fig. 3 Spectral functions of continuously changed gray-scaled intensity, from left to right: vertical orientation, corner-to-corner change, middle-centered. Topothesy for each case is comparable, while for the middle-centered case, the spectral function reveals a clear maximum value.

3 Results

Images have been obtained with the use of the Orion Plus Helium Ion Microscope (HIM) by Carl Zeiss Jena (Germany) using 34.2 kV acceleration voltage and 0.1-0.2 pA beam current [15]. The images are given in Fig. 4. The coding of names, 1-A, 1-D, 2-B, and 2-D, results from our internal convenience. The sizes of tested areas are equal to 27 μm x 27 μm and 135 μm x 135 μm , for samples (1-A, 1-D), and (2-B, 2-D), respectively. The choice of structures was determined by the aim to show the universality of the method. The first two samples represent the pattern of clearly visible fibers. The other two show the

fibers with less magnification and a more general perspective, which is suitable, e.g., for detection of stains or other contaminants.

From the technological point of view, sample 1-A is prepared from PAN on a polypropylene (PP) substrate, sample 1-D was additionally stabilized in a muffle oven, sample 2-B was also carbonized after stabilization, and finally sample 2-D was electrospun on an aluminum substrate, detached, stabilized and carbonized. Such choice of samples and microscopic magnification aims to show how topography is sensitive to such technological steps.

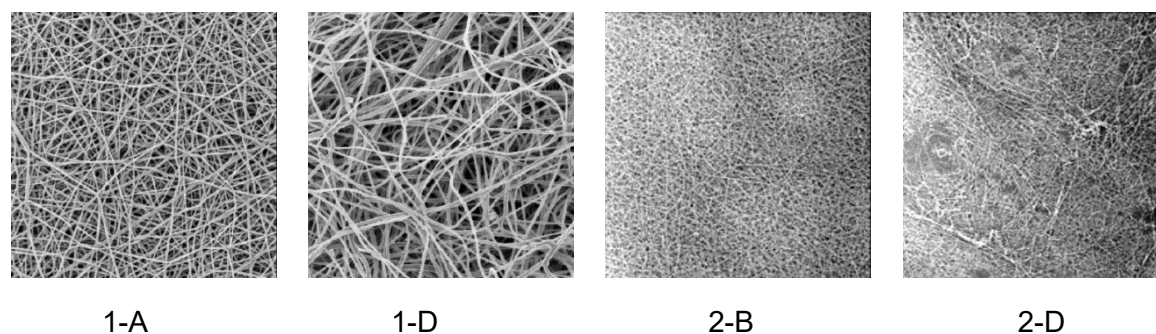


Fig. 4 Samples of PAN electrospun nanofiber mats for different technological steps of after-treatment (from left to right): poly(acrylonitrile) (PAN) on polypropylene (PP) (1-A), PAN on PP stabilized (1-D), PAN on PP stabilized and carbonized (2-B), PAN on aluminum substrate, detached, stabilized, and carbonized (2-D). The images should be compared in pairs: 1-A vs. 1-D, and 2-B vs. 2-D. All images are adopted from [15], originally published under a CC-BY license.

Details of spectral function calculations are given in Fig. 5 for sample 1-A. Firstly, the spectral function was calculated for a whole image (black frame), for 4 sub-images (red frames), and for 9 sub-images (blue frames). It is visible that the spectral function is dependent on the region under investigations. This does not change the fact that even one spectral function – calculated for a whole image – can be used as a fast check of surface quality.

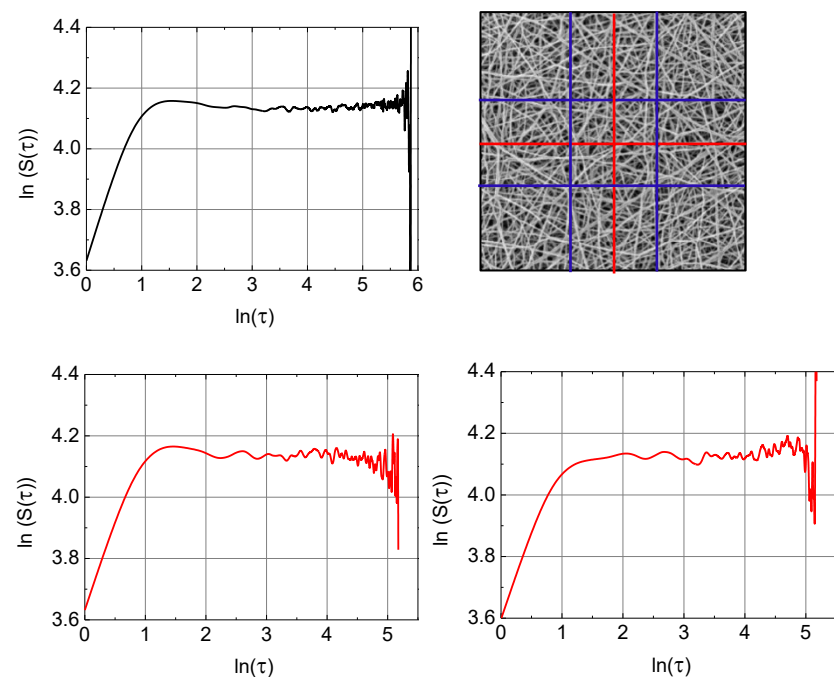


Fig. 5 Cont.

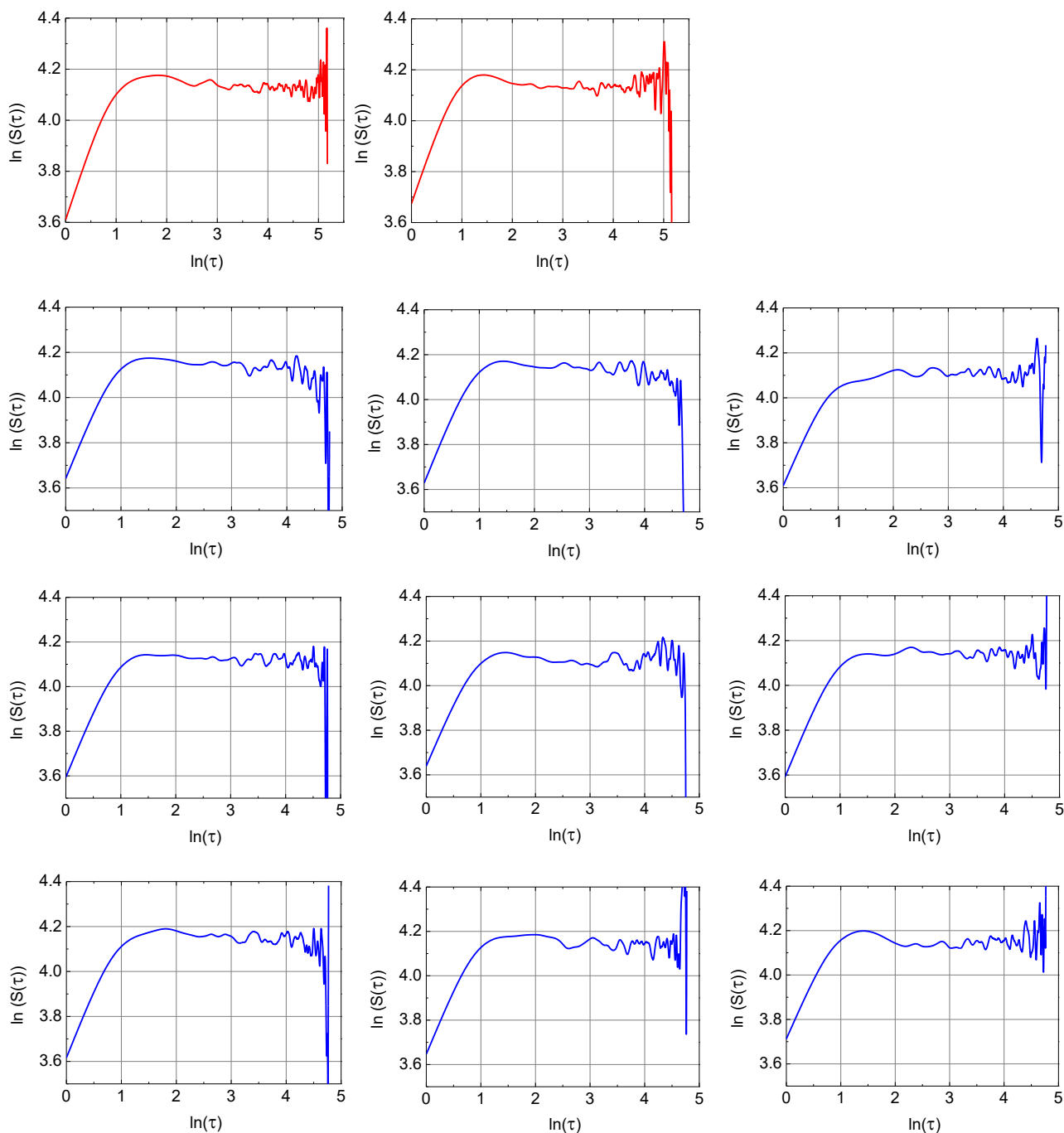


Fig. 5 Spectral functions for sample 1-A calculated for different sub-division of the original image. The HIM image is adopted from [15], originally published under a CC-BY license.

Results of all calculations are depicted in Figs. 6-9. We provide numerical values of toposy and the associated fractal dimension (comp. Eq. 4). Hence, it is interesting to compare obtained values of fractal dimensions with the capacity (d_{cap}) and correlation (d_{corr}) fractal dimensions, calculated separately for the whole image in our previous work [1]. At the top of each figure (Figs. 6-9), these values are additionally provided. It should be mentioned that the toposy, being a lengths scale, is here given in pixels, but could simply be translated into nanometers, taking into account the images' resolutions.

Sample 1-A, $d_{cap}=1.96$, $d_{corr}=1.90$ (**topothesy**/fractal dimension)

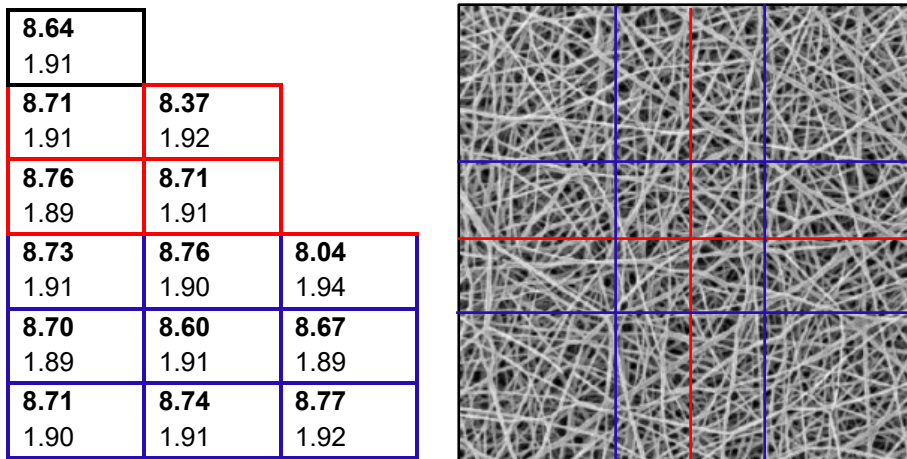


Fig. 6 *Topothesy and fractal dimension of sample 1-A for different regions of interest. The HIM image is adopted from [15], originally published under a CC-BY license.*

Sample 1-D, $d_{cap}=1.96$, $d_{corr}=1.77$ (**topothesy**/fractal dimension)

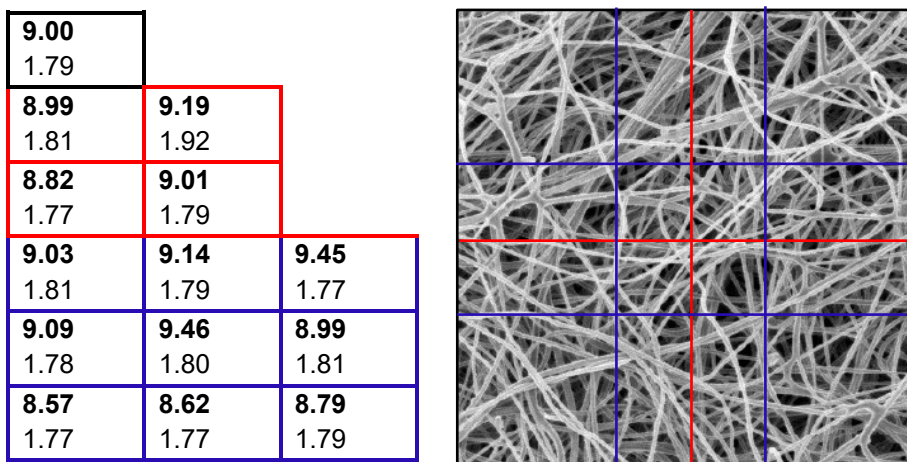


Fig. 7 *Topothesy and fractal dimension of sample 1-D for different region of interest. The HIM image is adopted from [15], originally published under a CC-BY license.*

Sample 2-B, $d_{cap}=1.93$, $d_{corr}=1.89$ (**topothesy**/fractal dimension)

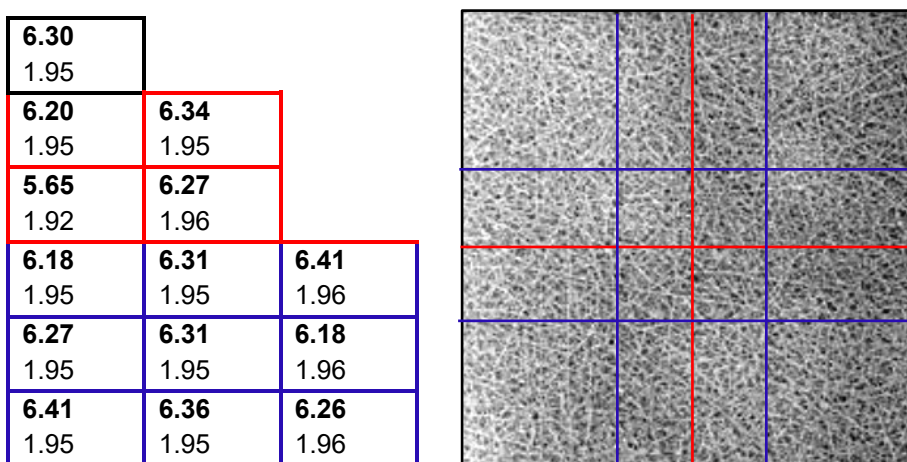


Fig. 8 *Topothesy and fractal dimension of sample 2-B, for different region of interest. The HIM image is adopted from [15], originally published under a CC-BY license.*

Sample 2-D, $d_{cap}=1.95$, $d_{corr}=1.84$ (**topothesy**/fractal dimension)

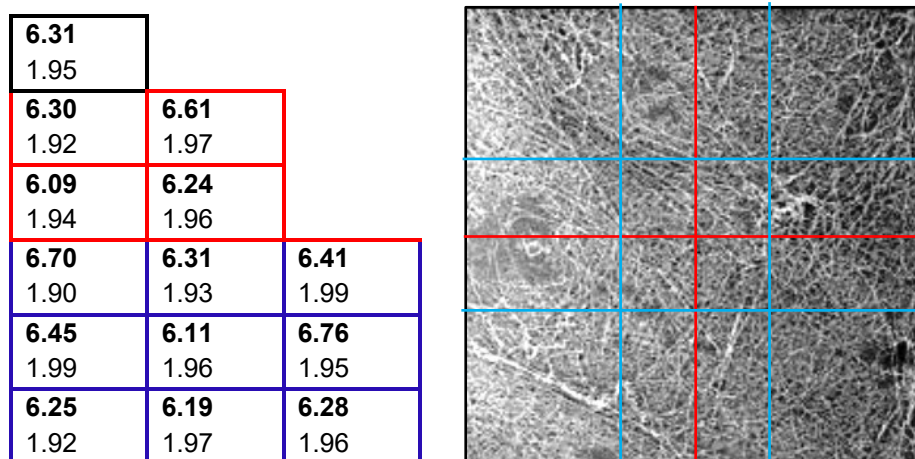


Fig. 9. Topothesy and fractal dimension of sample 2-D, for different region of interest. The HIM image is adopted from [15], originally published under a CC-BY license.

The obtained numerical data clearly classify the stabilization process, i.e., a transition from sample 1-A into sample 1-D. For a larger surface observation, the change in topothesy is not so evident. It is mostly detectable if to compare the 4-segmented images (red frames).

In order to test topothesy as a method for surface error detection, Fig. 10 shows two hypothetical situations, material loss and chemical stain. The tests were carried out with images of resolution 768 x 768 of sample 2-B. The obtained values of topothesy are equal to 6.52 and 6.23, respectively, while the original image at this resolution gave a topothesy of 6.63. Thus, the relative changes of topothesy for the cases of material loss and chemical stain are equal to 1.7 % and 6.0%, respectively.

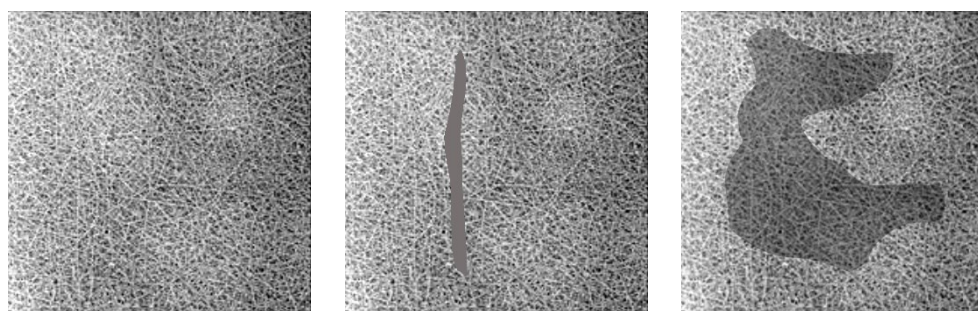


Fig. 10. Topothesy change of original sample (left panel) due to material loss (middle panel), and chemical stain (right panel); 6.63, 6.52, and 6.23, respectively. The original image is adopted from [15], originally published under a CC-BY license.

4 Conclusion

The topothesy parameter was obtained for gray-scaled images of different structures and magnifications. Obtained numerical values can be treated as the measure of surface complexity and a level of roughness. Especially, topothesy is more directly related to real surfaces than parameters calculated for black-and-white representation of samples.

Topothesy and fractal dimension were calculated for microscopic images of electrospun nanofiber mats after spinning and different thermal treatments. Interestingly, for larger magnifications, in which the internal structure is well seen, fractal dimension derived from topothesy are quantitatively similar to capacity fractal dimensions, as they can be calculated by a previously described method. On the other hand, for larger area observations, the topothesy-related fractal dimension can be interpreted as the

capacity fractal dimension. Hence, such comparison with other fractal-based method may serve as a proof of the correctness of the applied numerical method leading to toposy values.

Toposy of spun materials with larger sizes of fibers will be larger. The methodology has good spatial resolution. It can be used for evaluation of uniformity of textile materials during practical situations, e.g. in the production process. From the computer science point of view, the calculation of toposy and fractal dimension is very fast and the results can be obtained within seconds, making this method highly attractive for large-throughput tests.

Future research efforts will concentrate on different magnifications and materials to test the universality of the method as well as its limitations. Hence, specific numerical values for a wide range of samples will be classified as a possible standard of toposy.

References

- [1] Andreychouk, V.; Blachowicz, T.; Domino, K. Fractal dimension of cave for exemplary gypsum cave-mazes of Western Ukraine. *Landform Analysis* 2013, 22, 3-8. DOI: <https://doi.org/10.12657/landfana.022.001>.
- [2] Ehrmann, A.; Blachowicz, T. (2017) Image Processing Techniques for Evaluation of Textile Materials. In: *Examination of Textiles with Mathematical and Physical Methods*. Springer, Cham. DOI: https://doi.org/10.1007/978-3-319-47408-3_7.
- [3] Melo de, R.H.C.; Conci, A. How succolarity could be used as another fractal measure in image analysis. *Telecommunication Systems* 2011, 52, 1643-1655. DOI: <https://doi.org/10.1007/s11235-011-9657-3>.
- [4] Grzybowski, J.; Blachowicz, T. Estimation of spatial distribution and symmetry of textile materials using lacunarity. *CDATP* 2020, 1, 180-185. DOI: <https://doi.org/10.25367/cdatp.2020.1>.
- [5] Hanmandlu, M.; Choudhury, D.; Dash, S. Detection of defects in fabrics using toposy fractal dimension features. *SIVIP* 2014, 9, 1521-1530. DOI: <https://doi.org/10.1007/s11760-013-0604-5>.
- [6] Thomas, T. R.; Rosén, B.-G.; Amini, N. Fractal characterisation of the anisotropy of rough surfaces. *Wear* 1999, 232, 41-50. DOI: [https://doi.org/10.1016/S0043-1648\(99\)00128-3](https://doi.org/10.1016/S0043-1648(99)00128-3)
- [7] Thomas, T. R.; Rosén, B.-G. Determination of the optimum sampling interval for rough contact mechanics. *Tribology International* 2000, 33, 601-610. DOI: [https://doi.org/10.1016/S0301-679X\(00\)00076-1](https://doi.org/10.1016/S0301-679X(00)00076-1).
- [8] Russ, J. C. Fractal geometry in engineering metrology. In: Mainsah, E.; Greenwood, J. A.; Chetwynd, D. G. (eds.), *Metrology and Properties of Engineering Surfaces*, Springer, Boston, MA. DOI: https://doi.org/10.1007/978-1-4757-3369-3_2.
- [9] Hanmandlu, M.; Mittal, N.; Vijay, R. A robust finger knuckle print authentication using toposy and fractal dimension. *Defence Science Journal* 2017, 67, 66-73. DOI: <https://doi.org/10.14429/dsj.67.9003>
- [10] Ngan, H. Y. T.; Pang, G. K. H.; Yung, N. H. C. Automated fabric defect detection—A review. *Image and Vision Computing* 2011, 29, 442-458. DOI: <https://doi.org/10.1016/j.imavis.2011.02.002>.
- [11] Militký, J.; Bajzík, V. Surface roughness and fractal dimension. *The Journal of the Textile Institute* 2001, 92, 91-113. DOI: <https://doi.org/10.1080/00405000108659617>.
- [12] Blachowicz, T.; Böhm, T.; Grzybowski, J.; Domino, K.; Ehrmann, A. Analysis of AFM images of nanofibre mats for automated processing. *Tekstilec* 2020, 63, 104-112. DOI: <https://doi.org/10.14502/Tekstilec2020.63.94-103>.
- [13] Conci, A.; Proenca, C. B. A comparison between image-processing approaches to textile inspection. *The Journal of The Textile Institute* 2000, 91, 317-323. DOI: <https://doi.org/10.1080/00405000008659509>.
- [14] Javed, A.; Mirza, A. U. Comparative analysis of different fabric defects detection techniques. *I. J. Image, Graphics and Signal Processing* 2013, 1, 40-45. DOI: <https://doi.org/10.5815/ijigsp.2013.01.06>.
- [15] Storck, J. L.; Hellert, Ch.; Brockhagen, B.; Wortmann, M.; Diestelhorst, E.; Frese, N.; Grothe, T.; Ehrmann, A. Metallic supports accelerate carbonization and improve morphological stability of polyacrylonitrile nanofibers during heat treatment. *Materials* 2021, 14, 4686. DOI: <https://doi.org/10.3390/ma14164686>.
- [16] Russ, J. C. *Fractal surfaces*, Plenum Press, New York 1994.